ACS OMEGA

http://pubs.acs.org/journal/acsodf

Article

Mixed-Ligand Strategy for the Creation of Hierarchical Porous ZIF-8 for Enhanced Adsorption of Copper Ions

Zineb Latrach, Elmehdi Moumen, Said Kounbach, and Samir El Hankari*

Cite This: *ACS Omega* 2022, 7, 15862−15869

Read Online

ACCESS | Metrics & More | Article Recommendations | Supporting Information

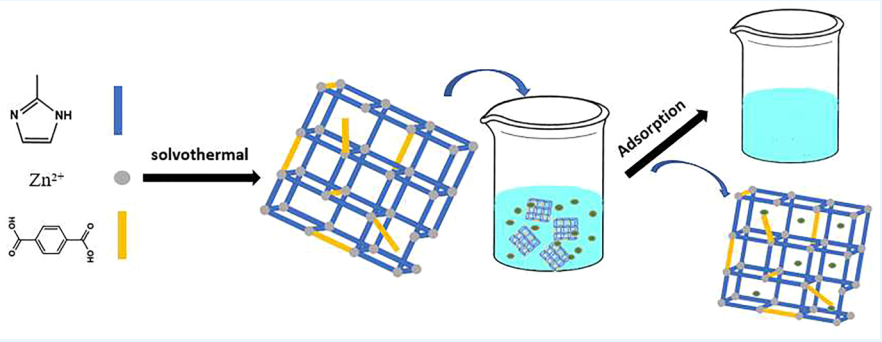

ABSTRACT: The adsorption of heavy metals using metal−organic framework-based adsorption technology has been pointed out as a promising technique for the removal of these toxic elements from water. However, their adsorption capacity needs to be enhanced. Thus, the current work reports the effect of using a mixed-ligand strategy on the MOF framework and its effect on the removal of copper ions from water by adding terephthalic acid (BDC) linker to the ZIF-8precursors (2-methylimidazole (mI) and Zn^{2+}) under solvothermal synthesis, leading to the formation of a hierarchical microporous mesoporous MOF, named Zn-mI-BDC, which was characterized by SEM, EDX, XRD, TGA, BET, and FTIR. As a result, all of these techniques revealed that the addition of a controlled amount of BDC did not alter the crystallinity of ZIF-8, resulting in the creation of a pore size of 4.2 nm. The new hierarchical porous MOF was tested for the adsorption of copper and exhibited an enhanced adsorption capacity compared to pristine ZIF-8 and many other standard adsorbents. The adsorption isotherm matched well with the Langmuir isotherm model, suggesting that the adsorption process chemisorption had a dominant role in the adsorption of Cu^{2+} species. Therefore, the current work is considered as an important step toward the use of a mixed-ligand strategy in enhancing the adsorption capacity of heavy metals using MOF materials.

INTRODUCTION

During the past two decades, extensive work has been performed on the synthesis and study of materials known as metal−organic frameworks (MOFs), which have emerged as a new family of crystalline hybrid organic/inorganic porous materials with outstanding performance in various potential applications including catalysis,[1,2] adsorption,[3−5] sensing,[6] and so on,[7−10] due to their fascinating properties such as ultrahigh surface area, tunable porosity, and excellent thermal and chemical stability.[11−13] However, in some cases, their micro-sized pores and narrow channels inherently restrict their adsorption capacity.[11,14,15]

For example, Yaghi et al. reported zeolitic imidazolate frameworks (ZIFs) with a high surface area and high thermal and water stability with small pores since the organic linker is imidazole.[16] For this reason, strategies to enhance the adsorption performance of MOFs are needed. In this context, different approaches have been investigated to create defects in MOFs with accessible active sites to boost their adsorption capacity for heavy metals, particularly copper ions.[17] Building MOFs with different ligands or different metals for the synthesis of mixed-ligand or mixed-metal MOFs, respectively, could generate more defects and larger pore sizes.[18−21]

Water is a vital element in life which is used for several human needs and activities such as drinking, domestic use, and food production.[22] Despite intensive efforts, access to safe drinking water is still at risk owing to the intolerable amounts of heavy metals found in numerous water streams and food webs.[23] However, heavy metals released from industrial activities and daily use are a major concern for the environmental ecosystem which can engender adverse health

Received: February 17, 2022
Accepted: April 13, 2022
Published: April 25, 2022

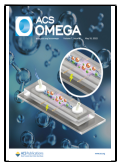

https://doi.org/10.1021/acsomega.2c00980
ACS Omega 2022, 7, 15862−15869

effects on humans, animals, plants, and microorganisms.[23] For instance, copper is one of the most widely used heavy metals in many industrial sectors, such as electric and electronic applications as well as industries of alloys, paints, and agriculture, etc.[23] This chemical element is toxic even at low doses for many organisms, especially in aquatic environments.[23] Accordingly, effective solutions for the efficient remediation of trace copper from water are key alternatives to promote environmental and human well being. Indeed, various adsorbents have been used in the removal of copper such as activated carbon,[24] zeolite,[25] and biochar.[26] However, these conventional adsorbents suffer from low adsorption capacity and modest removal efficiency due to their low surface area and limited adsorptive sites. Therefore, designing and synthesizing a new adsorbent is quite important for the development of a significant adsorption technology for the removal of toxic metals from aquatic systems.

Mixed-ligand MOFs offer many opportunities for the creation of functional active sites, which can effectively enhance the adsorption efficiency of these materials. Herein, a ZIF-8 material (Zn-mI) was chosen as a model for our study, as it was employed previously in the removal of copper species,[27] and a mixed-ligand MOF strategy was chosen to demonstrate the proof of this concept in accessing more active sites and large cavities to improve the diffusion and mass transfer and thus enhance the adsorption efficiency of ZIF-8 for copper removal from water. Dicarboxylic benzene acid (H_2BDC) was added as a second ligand to form a new mixed-ligand MOF material (Zn-mI-BDC), which was used for the adsorption of Cu^{2+}, and subsequently compared to pristine ZIF-8 under the same working conditions. The Langmuir model, Freundlich model, and pseudo-first order kinetics, and pseudo-second order kinetics were used to describe the adsorption behaviors.

RESULTS AND DISCUSSION

Characterization of Zn-mI-BDC and ZIF-8. The XRD patterns of pristine ZIF-8 and mixed-ligand Zn-mI-BDC materials are displayed in Figure 1. While the pristine ZIF-8 shows eight main characteristics peaks at 2 tetha of 7° and 3°, 10° and 4°, 12° and 7°, 14° and 7°, 16° and 4°, 18° and 1°, 24° and 5°, and 26° and 7° typical for the ZIF-8 material,[27] Zn-mI-BDC exhibits the same peaks as pristine ZIF-8, confirming that the addition of a controlled amount of H_2BDC did not alter the crystallinity of our synthesized ZIF-8. The small additional peaks at 8° and 9°, 11° and 1°, 17° and 1°, and 17° and 5° can be attributed to the coordination framework between terephthalic acid (BDC) and Zn (Zn−BDC).[28] This interference of the coordination between BDC and mI on the Zn cluster can create some defects within the new material, leading to the creation more active sites.

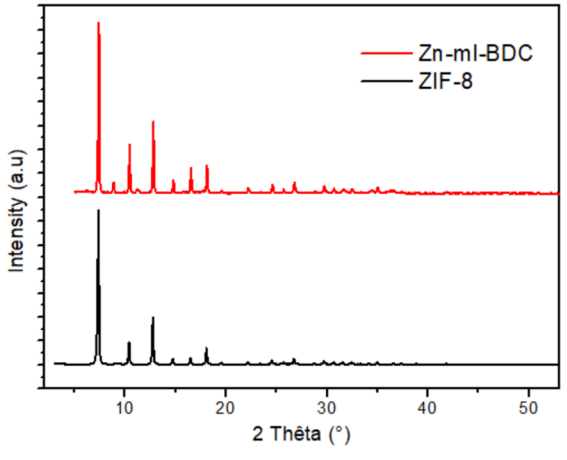

Figure 1. X-ray diffraction patterns of ZIF-8 and Zn-mI-BDC.

It is well known that the pore size distribution and specific surface area of the adsorbent have an important effect on its adsorption performance. N_2 adsorption−desorption isotherms were carried out, and the results are recorded in Figure 2. The curve of ZIF-8 shows that the N_2 adsorption−desorption isotherm is type I. Although Zn-mI-BDC exhibited a N_2 adsorption−desorption isotherm of type I, a hysteresis loop was observed which is typical for a hierarchical microporous and mesoporous material (Figure 2a).[29]

The isotherm profile indicates that Zn-mI-BDC is a hierarchical microporous mesoporous material with a specific surface area of 1106 m^2/g and a narrow pore size of 4.2 nm (calculated by the BJH desorption), while ZIF-8 is a microporous material (<2 nm) with a specific surface area of 1477 m^2/g (Table 1 and Figure 2b), which confirms the creation of mesopores after adding the second ligand.

The morphology of the synthesized materials was characterized with scanning electron microscopy (SEM) as shown in Figure 3a and 3b. The synthesized ZIF-8 has a typical rhombic dodecahedral shape with a particle diameter of ∼122 μm, similar to that reported in the literature.[30,31] However, a decrease in the crystal size from 100−122 to 30−60 μm was observed after adding H_2BDC with the appearance of more broken pieces, proving that the addition of a second ligand constrains the normal growth of ZIF-8 crystals.

In order to identify the elemental composition of ZIF-8 and Zn-mI-BDC, energy-dispersive X-ray analysis (EDX) was performed in parallel with SEM characterization (Figure 4a and 4b). As it can be seen, zinc, azote, carbon, and oxygen are present in both materials. In addition, the elemental composition of the mixed-ligand Zn-mI-BDC was almost identical with the pristine ZIF-8 since the added ligand (BDC) was just 10%; a slight increase of oxygen atoms was observed due to the presence of carboxylate groups in the BDC ligand, while a minor decrease in azote was noted due to the decrease of mI ligands (Figure 4b).

To determine the quantity of BDC incorporated in the framework and reveal the thermal stability of these porous compounds. Both MOFs were subjected to thermogravimetric analysis (TGA), and the results are presented in Figure 5. The TGA curve of the as-synthesized sample of ZIF-8 exhibited two gradual weight-loss steps: the first one corresponding to the removal of guest molecules (mainly H_2O) from the cavities, and the second one is associated with a long plateau in the temperature range of 400−600 °C, indicating the high thermal stability of ZIF-8. On the other hand, the TGA curve of Zn-mI-BDC was comprised of three stages, and the thermal decomposition of Zn-mI-BDC began at about 200 °C. While the first stage was due to the removal of water molecules at temperatures under 200 °C, the second stage between 200 and 370 °C resulted from the decomposition of BDC groups since it corresponds to a weight loss of ∼10% as introduced in the experimental part. The third stage was because of the decomposition of 2-methyl imidazole of the MOF, and there is a loss of 64% by weight. The thermal stability of Zn-mI-BDC

https://doi.org/10.1021/acsomega.2c00980
ACS Omega 2022, 7, 15862−15869

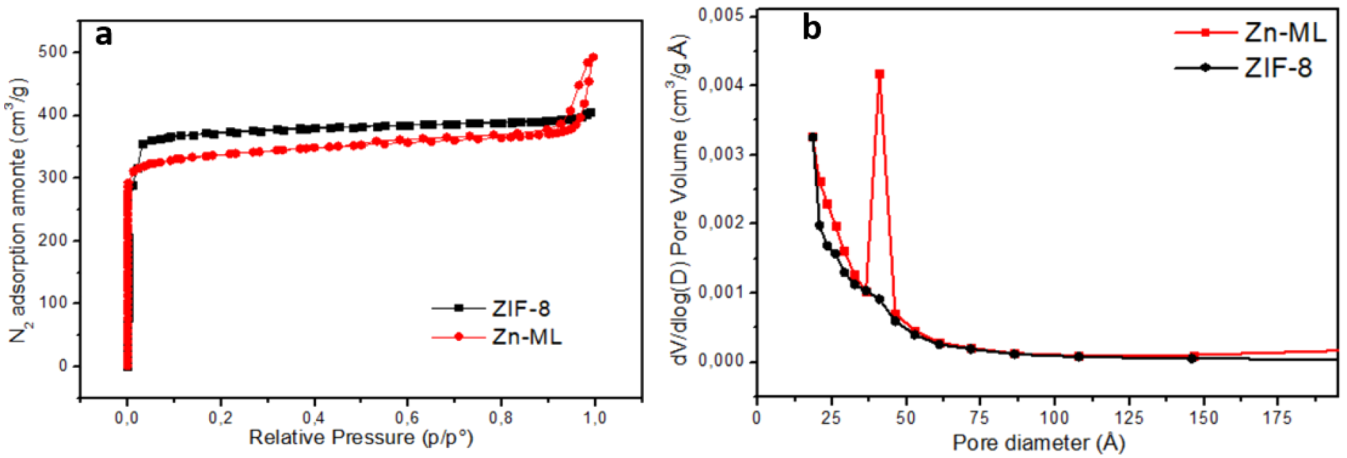

Figure 2. (a) N_2 adsorption−desorption isotherms and (b) pore-size distributions of ZIF-8 and Zn-mI-BDC materials.

Table 1. Textural Properties of ZIF-8 and Zn-mI-BDC

samples	pore size (nm)	S_{BET} (m^2/g)	V_{micro} (cm^3/g)	V_{total} (cm^3/g)
ZIF-8	<2	1477.2	0.52	0.63
Zn-mI-BDC	4.2	1106.9	0.44	0.803

was slightly lower than that of ZIF-8, which is attributed to the creation of defects.[32]

Further evidence to characterize the functional groups of ZIF-8 and mixed-ligand MOF Zn-mI-BDC was provided by Fourier-transform infrared (FTIR) spectroscopy. The FTIR spectra of ZIF-8, coordinated ligands, terephthalic acid (H_2BDC), and 2-methyl imidazole (2-mI) are shown in Figure 6. As observed, 2-methylimidazole exhibits a broad and strong absorption in the range of 2200−3250 cm^{-1} due to vibrations of the hydrogen bonds established between the pyrrole group and the pyridinic nitrogen (N−H···N). Also, N−H stretching vibrations can be observed as well at 1849 cm^{-1},[33] which completely disappeared in the ZIF-8 and Zn-mI-BDC spectra, indicating that the 2-mI ligands are fully reacted during formation of both MOFs. Besides, the band at 1584 cm^{-1} represents the stretching vibration of C═N. In addition, all vibrational modes of ZIF-8 are present in the infrared spectra of the Zn-mI-BDC material, which indicates that the addition of BDC did not change the functional groups of ZIF-8. However, the appearance of vibrational modes in the infrared spectra of Zn-mI-BDC such as those at 1669 and 1396 cm^{-1}, which are related to the asymmetric and symmetric stretching modes of coordinated carboxylic acid, respectively, indicates the attachment of a carboxylate group of BDC in the mixed-ligand MOF.

In an attempt to further investigate the charge state of ZIF-8 and Zn-mI-BDC particles, zeta potential measurements across a wide pH range were conducted (Figure 7). Both ZIF-8 and Zn-mI-BDC demonstrated a positive zeta potential in acidic pH and then flipped to a negative zeta potential at pH values of 3.7 and of 4.2 for Zn-mI-BDC and ZIF-8, respectively. The value of the point of zero charge implied that the surface charge of Zn-mI-BDC particles was positive when the pH of the solution is lower than 3.7; then, it is reversed into negative charge at a pH greater than 3.7.

Heavy Metal Adsorption Study. MOFs are typically porous materials; their excellent properties for the removal of metal ions are due to the presence of pores and active adsorptive sites in their frameworks.[34] In this work, we synthesized a mixed-ligand Zn-mI-BDC adsorbent with more

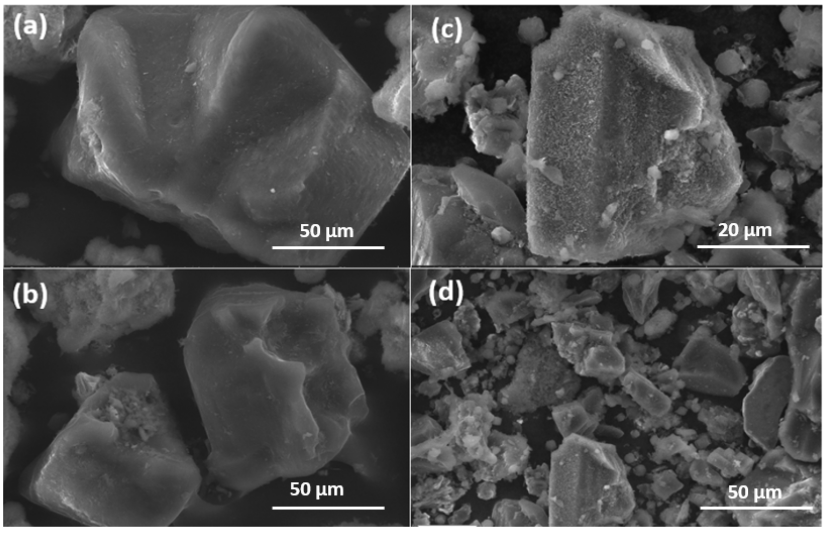

Figure 3. SEM images of normal ZIF-8 (a, b) and Zn-mI-BDC (c, d).

https://doi.org/10.1021/acsomega.2c00980
ACS Omega 2022, 7, 15862−15869

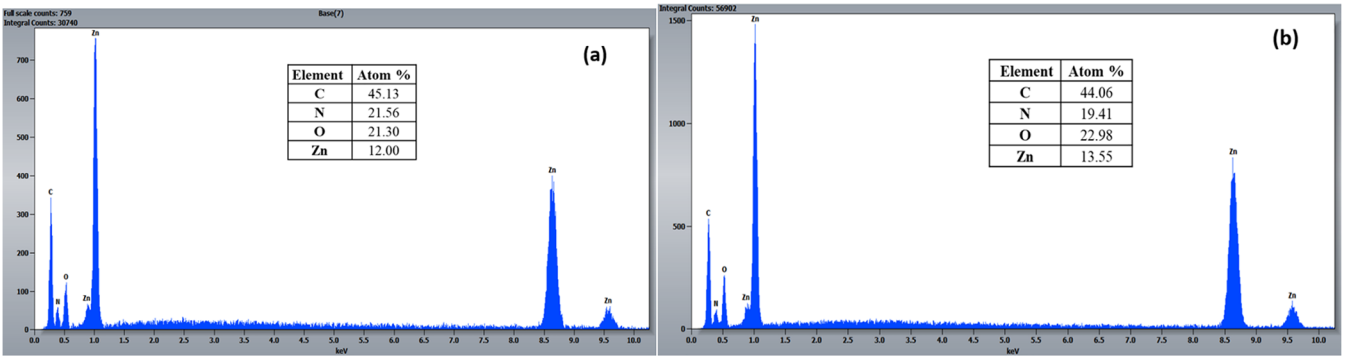

Figure 4. Energy-dispersive X-ray analysis for ZIF-8 (a) and Zn-mI-BDC (b).

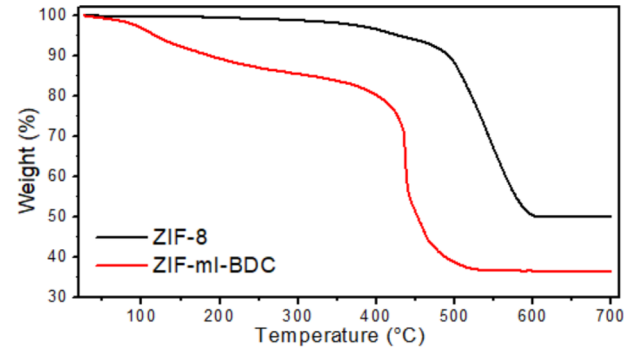

Figure 5. TGA curves of ZIF-8 and Zn-mI-BDC.

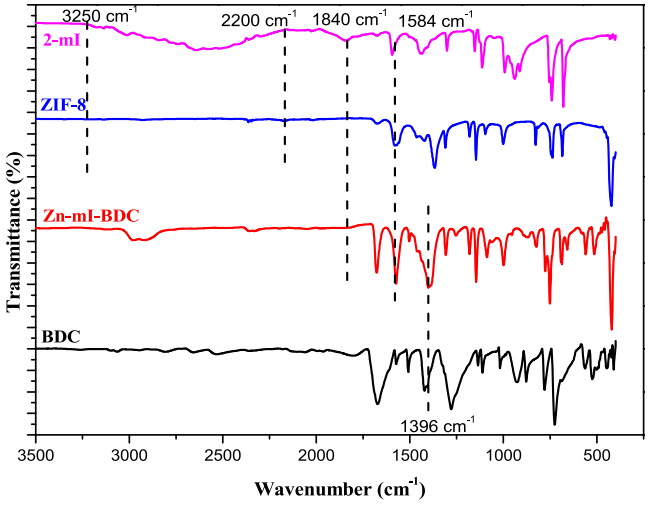

Figure 6. FTIR spectra of 2-mI, BDC, ZIF-8, and Zn-mI-BDC.

accessible sites and investigated its adsorption ability for the removal of copper from aqueous solution.

Effect of Different Parameters Affecting the Adsorption. The adsorption capacity for Cu^{2+} on Zn-mI-BDC is shown in Figure 8. It can be seen that the adsorption of copper is obviously improved after adding the BDC ligand, presumably due to increased adsorption sites and the presence of mesopores that promoted access to these active sites, which all together play an important role in improving the Zn-mI-BDC adsorption efficiency.

The effect of contact time on Cu^{2+} ion removal was also studied. As expected, Figure 8a shows that the rate of adsorption increases as the contact time increases. Also, the Cu^{2+} removal rate was faster using Zn-mI-BDC and higher

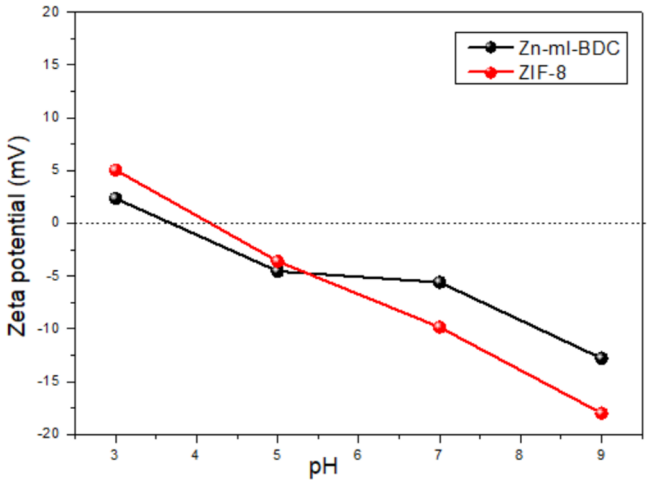

Figure 7. Zeta potential measurements for Zn-mI-BDC and ZIF-8 at different pH values.

when compared to that of ZIF-8. Thereby, in the first 5 min, Zn-mI-BDC removed 47% of Cu^{2+} while ZIF-8 adsorbed only 29%. Besides, the removal rate for both MOFs was rapid at the beginning, which could be explained by the availability of pores and the number of active sites at the beginning of the adsorption process.[27] Thereafter, the number of active sites was reduced, thus decreasing the removal rate.

The effect of Cu^{2+} concentration on the mixed-ligand MOF Zn-mI-BDC was also investigated. Figure 8b shows the effect of the initial concentration on the removal of copper ions on Zn-mI-BDC and its adsorption capacity. The results demonstrated that the removal performance decreased gradually with increasing copper concentration. This was attributed to saturation of available active sites, indicating that Zn-mI-BDC did not provide enough binding sites to adsorb all of the Cu^{2+} ions in the highly concentrated solution.[17] Furthermore, the adsorption efficiency was positively related to temperature (Figure S1), as higher temperatures are expected to provide enough energy to accelerate the diffusion of copper ions into the pores of the adsorbent.[27] In addition, the increase of copper removal at higher temperatures indicates that the adsorption of Cu^{2+} ions on Zn-mI-BDC is an endothermic process.[35]

Adsorption Isotherm and Adsorption Kinetic Models. The correlation between the amount of Cu(II) ions adsorbed onto the mixed-ligand MOF Zn−Cu−BDC and the equilibrium concentration of Cu(II) ions was estimated using Langmuir and Freundlich isotherm models (Text S1).[27,36]

https://doi.org/10.1021/acsomega.2c00980
ACS Omega 2022, 7, 15862−15869

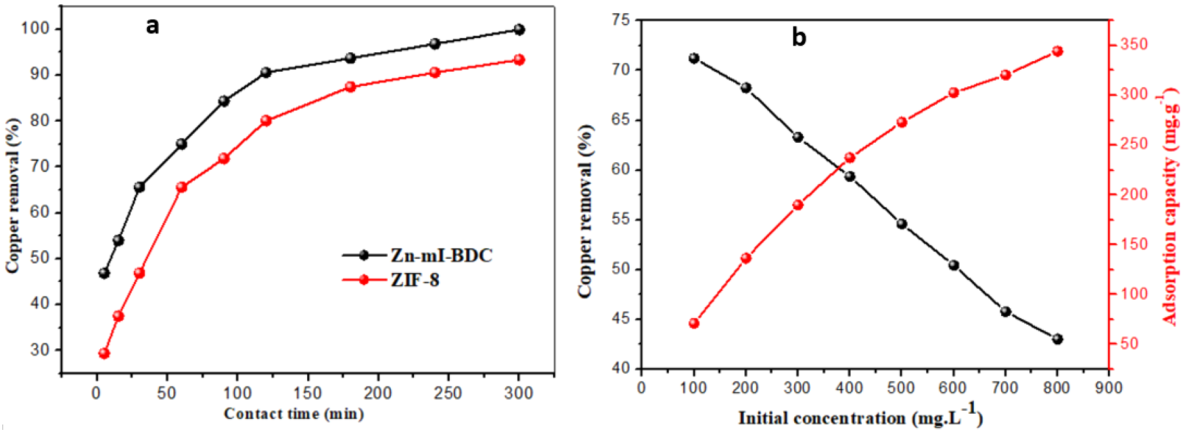

Figure 8. (a) Effect of contact time on the removal of copper by Zn-mI-BDC and ZIF-8 ([Cu^{2+}] = 200 mg/L; adsorbents = 5 mg; V = 10 mL; $T°$ = 298 K). (b) Effect of initial concentration on the removal of copper on Zn-mI-BDC and its adsorption capacity ([Cu^{2+}] = 200 mg/L; adsorbents = 5 mg; V = 10 mL; contact time: 60 min; pH = 5; $T°$ = 298 K).

Batch experiments were carried out with different initial copper concentrations (100−800 mg·L^{-1}) at room temperature over 1 h.

The linear plots of the Langmuir (Figure S2a) and Freundlich (Figure S2b) models were studied, and their related relative parameters were determined (Table S1). As a result, the Langmuir isotherm model was found to be linear over the entire concentration range with a good linear correlation coefficient (R^2 = 0.9980), which is higher than that of the Freundlich model (R^2 = 0.9726), indicating that the Langmuir equation represents the best fit of the experimental data. Also, the process occurs on a heterogeneous surface, and the calculated R_L values (Text S1) for the studied concentrations are all between 0 and 1 (0.15 and 0.58), which revealed an efficient adsorption process. In addition, n was greater than 1, demonstrating the high affinity of Zn-mI-BDC for copper. The nonlinear plots of the Langmuir and Freundlich models (Figure 3c) and their related parameters (Table S1) exhibited primarily the same results of that of the linear fit.

The adsorption kinetics of copper on Zn-mI-BDC were explored as well, not only to study the rate of adsorption but also to evaluate the adsorption efficiency. In this regard, pseudo-first-order and pseudo-second-order kinetics models were used to confirm the relation between adsorption and time (Text S2).[37] Accordingly, pseudo-second-order kinetics was more appropriate to describe the adsorption process since the correlation coefficient R_2^2 was higher (R_2^2 = 0.9977 > R_1^2 = 0.9610) and the calculated Q_e (Q_e = .197) was closer to that of the measured data (Q_{eexp} = 0.189) (Text S2, Figure S3, and Table S2). Therefore, these results suggest that the adsorption process is subjected to a pseudo-second-order kinetic model which assumes a chemical adsorption process. Thus, the adsorption may not be fully reversible and requires more effort for material regeneration.[37]

In addition, a comparison of the adsorption capacity between our newly developed hierarchical porous Zn-Im-BDC adsorbent with pristine ZIF-8 and other reported adsorbents is given in Table 2. The adsorption capacity of Zn-Im-BDC (200 mg·g^{-1}) is superior to or identical with most of the reported adsorbents, indicating that the designed adsorbent holds great promise in copper treatment from water and that more hierarchical porous MOFs can be prepared and used for the removal of Cu^{2+} and other heavy metals.

Table 2. Copper Adsorption Data Using Various Adsorbents

adsorbent	adsorption capacity (mg·g^{-1})	pH	equilibrium time (min)	ref
Zn-mI-BDC	200	6.8	100	this work
ZIF-8	116.98	5	30	27
Cu-ZIF-8	135.12	4−6		38
MOF-5	290	5.2	60	39
Ag−Fe MOF	213	5	65	17
carbon foam	246.66	6−7	1440	40
Activated carbon	43.47	5	180	24
PGCB	100	5	180	41
PNIPAM-Co-AA	67.25	5		42
keratin/PA6 nanofibers	103.5	5.8	300	43

CONCLUSIONS

In this study, a hierarchical microporous mesoporous MOF, Zn-mI-BDC, was successfully synthesized using a mixed-ligand MOF strategy by adding terephthalic acid and 2-methylimidazole (mI) linkers. It was revealed that the addition of a controlled amount of a second ligand did not alter the crystallinity of ZIF-8 and interestingly resulted in the creation of larger pores and shrunken size in morphology, leading to an enhanced adsorption capacity of Cu^{2+} compared to pristine ZIF-8. Moreover, the maximum adsorption capacity was better than many existing adsorbents. The adsorption of Cu^{2+} using Zn-mI-BDC fitted well with both linear and nonlinear pseudo-second-order models, and the adsorption isotherm matched well with the Langmuir isotherm model, suggesting that the adsorption process was controlled by chemical reactions. Therefore, this work will inspire other researchers who further attempt to improve heavy metal adsorption using metal−organic frameworks.

EXPERIMENTAL SECTION

Chemicals. The chemicals used in the study were of analytical grade and used without any further purification. Zinc nitrate hexahydrate ($Zn(NO_3)_2·6H_2O$), 2-methylimidazole (mI), terephthalic acid (H_2BDC), copper sulfate anhydrous ($CuSO_4$), sodium hydroxide (NaOH), *N*,*N*-dimethylformamide (DMF), ethanol, and acetone were received from Sigma-Aldrich.

https://doi.org/10.1021/acsomega.2c00980
ACS Omega 2022, 7, 15862−15869

ZIF-8 Synthesis. ZIF-8 was prepared according to the literature procedure with some modifications.[44] Briefly, zinc nitrate hexahydrate (1.78 g) and 2-methylimidazole (0.49 g) were completely dissolved in 60 mL of DMF and stirred vigorously until a clear solution was obtained. Then, the mixture was introduced to a 100 mL bottle with a Teflon-taped screw cap and heated at 140 °C for 24 h in a convection oven. Eventually, the product was centrifuged, washed with DMF several times, kept in MeOH for 3 days to remove the remaining DMF in the pores, and dried at room temperature.

Zn-mI-BDC Mixed-Ligand MOF Synthesis. Zn-mI-BDC was synthesized using H_2BDC and mI linkers; the molar ratio of H_2BDC/mI was 0.9:0.1. Typically, 2.009 g of zinc nitrate hexahydrate (6.756 mmol), 0.501 g of 2-methylimidazole (6.102 mmol), and 0.101 g of H_2BDC (0.609 mmol) were completely dissolved in 60 mL of DMF and stirred vigorously until a clear solution was obtained. Then, the mixture was introduced to a 100 mL bottle with a Teflon-taped screw cap and heated at 140 °C for 24 h in a convection oven. Eventually, the product was centrifuged, washed with DMF several times, kept in MeOH for 3 days, and dried at room temperature.

Characterization. The physicochemical properties of both MOFs (Zn-mI-BDC and ZIF-8) were characterized with a series of analytical methods. X-ray diffraction (XRD) measurements were performed using a D8 Advance X-ray diffractometer. The crystal size and particle morphology of the materials were examined by scanning electron microscopy (SEM) (operated at 20 kV, QUATTRO S-FEG-ThermoFisher Scientific). Energy-dispersive X-ray analysis (EDX) was investigated in parallel with SEM analysis. Thermal analysis was carried out under an air atmosphere at a rate of 10 °C/min over the range of 25−700 °C (TA DSC Q20). A JASCO FTIR-4600 spectrometer was used to record the FTIR spectra from 400 to 4000 cm^{-1}. The Brunauer−Emmett−Teller (BET) surface area, pore size, and the pore volume were measured with a gas sorption analyzer (Micromeritics 3-Flex Surface Characterization Analyzer). The zeta potential of the materials was measured using a Zetameter (Zetasizer Nano ZS90, Malvern) at room temperature. A simultaneous inductively coupled plasma atomic emission spectrometer ICP-AES (PerkinElmer Avio 500) was used to determine the copper concentration in aqueous solutions.

Batch Adsorption Experiments. Multiple batch adsorption tests were managed to investigate the adsorption performance of the developed MOF adsorbents. For this reason, an aqueous solution of copper with different concentrations was used to carry out the adsorption experiments. In brief, 20 mg of MOF as the adsorbent was introduced to each tube containing 5 mL of copper ions, which was well mixed and kept at room temperature. Subsequently, the solution was separated from the adsorbent via centrifugation and filtration. The content of copper in the solution was measured by ICP-AES. Batch adsorption results were the average values of three replicate experiments.

In general, the removal efficiency ($R\%$) and adsorption capacity Q_e (mg/g) of the copper ions were determined according to eqs 1 and 2, respectively

$$R\% = \frac{C_0 - C_e}{C_0} \quad (1)$$

$$Q_e = (C_0 - C_e)\frac{V}{m} \quad (2)$$

where C_0 ($mg{\cdot}L^{-1}$) and C_e ($mg{\cdot}L^{-1}$) are the initial and equilibrium concentrations of the adsorbate in solution, respectively, V (mL) is the volume of the solution, and m (g) is the mass of the adsorbent.

■ ASSOCIATED CONTENT

Supporting Information

The Supporting Information is available free of charge at https://pubs.acs.org/doi/10.1021/acsomega.2c00980.

Adsorption isotherm; adsorption kinetics; effect of temperature on the removal of copper by Zn-mI-BDC; linear and nonlinear Langmuir and Freundlich adsorption isotherms; pseudo-first-order kinetics and pseudo-second-order kinetics; Langmuir and Freundlich data for copper adsorption on Zn-mI-BDC; kinetic results for copper adsorption by Zn-mI-BDC (PDF)

■ AUTHOR INFORMATION

Corresponding Author

Samir El Hankari − *Chemical and Biochemical Sciences, Green Process Engineering, Mohammed VI Polytechnic University (UM6P), 43150 Ben Guerir, Morocco;* orcid.org/0000-0002-9123-6857; Email: samir.elhankari@um6p.ma

Authors

Zineb Latrach − *Chemical and Biochemical Sciences, Green Process Engineering, Mohammed VI Polytechnic University (UM6P), 43150 Ben Guerir, Morocco*

Elmehdi Moumen − *Chemical and Biochemical Sciences, Green Process Engineering, Mohammed VI Polytechnic University (UM6P), 43150 Ben Guerir, Morocco*

Said Kounbach − *Chemical and Biochemical Sciences, Green Process Engineering, Mohammed VI Polytechnic University (UM6P), 43150 Ben Guerir, Morocco*

Complete contact information is available at: https://pubs.acs.org/10.1021/acsomega.2c00980

Notes

The authors declare no competing financial interest.

■ ACKNOWLEDGMENTS

The authors acknowledge the financial support from the Laboratory of Chemical and Biochemical Sciences, Green Process Engineering of Mohammed VI Polytechnic University (UM6P).

■ REFERENCES

(1) Moumen, E.; Assen, A. H.; Adil, K.; Belmabkhout, Y. Versatility vs Stability. Are the Assets of Metal − Organic Frameworks Deployable in Aqueous Acidic and Basic Media ? *Coord. Chem. Rev.* **2021**, *443*, 214020.

(2) Bavykina, A.; Kolobov, N.; Khan, I. S.; Bau, J. A.; Ramirez, A.; Gascon, J. Metal-Organic Frameworks in Heterogeneous Catalysis: Recent Progress, New Trends, and Future Perspectives. *Chem. Rev.* **2020**, *120* (16), 8468−8535.

(3) Moumen, E.; Bazzi, L.; El Hankari, S. Aluminum-Fumarate Based MOF: A Promising Environmentally Friendly Adsorbent for the Removal of Phosphate. *Process Saf. Environ. Prot.* **2022**, *160*, 502−512.

(4) Bazzi, L.; Ayouch, I.; Tachallait, H.; EL Hankari, S. Ultrasound and Microwave Assisted-Synthesis of ZIF-8 from Zinc Oxide for the Adsorption of Phosphate. *Results Eng.* **2022**, *13* (March), 100378.

(5) El-Hankari, S.; Aguilera-Sigalat, J.; Bradshaw, D. Surfactant-Assisted ZnO Processing as a Versatile Route to ZIF Composites and Hollow Architectures with Enhanced Dye Adsorption. *J. Mater. Chem. A* **2016**, *4* (35), 13509−13518.
(6) Moumen, E.; Bazzi, L.; El Hankari, S. Metal-Organic Frameworks and Their Composites for the Adsorption and Sensing of Phosphate. *Coord. Chem. Rev.* **2022**, *455*, 214376.
(7) Rocío-Bautista, P.; Taima-Mancera, I.; Pasán, J.; Pino, V. Metal-Organic Frameworks in Green Analytical Chemistry. *Separations* **2019**, *6* (3), 33.
(8) Kobielska, P. A.; Howarth, A. J.; Farha, O. K.; Nayak, S. Metal−Organic Frameworks for Heavy Metal Removal from Water. *Coord. Chem. Rev.* **2018**, *358*, 92−107.
(9) Agostoni, V.; Chalati, T.; Horcajada, P.; Willaime, H.; Anand, R.; Semiramoth, N.; Baati, T.; Hall, S.; Maurin, G.; Chacun, H.; Bouchemal, K.; Martineau, C.; Taulelle, F.; Couvreur, P.; Rogez-Kreuz, C.; Clayette, P.; Monti, S.; Serre, C.; Gref, R. Towards an Improved Anti-HIV Activity of NRTI via Metal-Organic Frameworks Nanoparticles. *Adv. Healthcare Mater.* **2013**, *2*, 1630−1637.
(10) El-Hankari, S.; Huo, J.; Ahmed, A.; Zhang, H.; Bradshaw, D. Surface Etching of HKUST-1 Promoted via Supramolecular Interactions for Chromatography. *J. Mater. Chem. A* **2014**, *2* (33), 13479−13485.
(11) Liu, D.; Zou, D.; Zhu, H.; Zhang, J. Mesoporous Metal−Organic Frameworks: Synthetic Strategies and Emerging Applications. *Small* **2018**, *14* (37), 1801454.
(12) Kuppler, R. J.; Timmons, D. J.; Fang, Q. R.; Li, J. R.; Makal, T. A.; Young, M. D.; Yuan, D.; Zhao, D.; Zhuang, W.; Zhou, H. C. Potential Applications of Metal-Organic Frameworks. *Coord. Chem. Rev.* **2009**, *253* (23−24), 3042−3066.
(13) Wang, F.; Xu, K.; Jiang, Z.; Yan, T.; Wang, C.; Pu, Y.; Zhao, Y. A Multifunctional Zinc-Based Metal-Organic Framework for Sensing and Photocatalytic Applications. *J. Lumin.* **2018**, *194*, 22−28.
(14) Bradshaw, D.; El-Hankari, S.; Lupica-Spagnolo, L. Supramolecular Templating of Hierarchically Porous Metal-Organic Frameworks. *Chem. Soc. Rev.* **2014**, *43* (16), 5431−5443.
(15) Hammi, N.; El Hankari, S.; Katir, N.; Marcotte, N.; Draoui, K.; Royer, S.; El Kadib, A. Polysaccharide Templated Biomimetic Growth of Hierarchically Porous Metal-Organic Frameworks. *Microporous Mesoporous Mater.* **2020**, *306* (June), 110429.
(16) Wang, B.; Côté, A. P.; Furukawa, H.; O'Keeffe, M.; Yaghi, O. M. Colossal Cages in Zeolitic Imidazolate Frameworks as Selective Carbon Dioxide Reservoirs. *Nature* **2008**, *453* (7192), 207−211.
(17) Abo El-Yazeed, W. S.; Abou El-Reash, Y. G.; Elatwy, L. A.; Ahmed, A. I. Novel Bimetallic Ag-Fe MOF for Exceptional Cd and Cu Removal and 3,4-Dihydropyrimidinone Synthesis. *J. Taiwan Inst. Chem. Eng.* **2020**, *114*, 199−210.
(18) Yin, X.; Alsuwaidi, A.; Zhang, X. Hierarchical Metal-Organic Framework (MOF) Pore Engineering. *Microporous Mesoporous Mater.* **2022**, *330*, 111633.
(19) Dhakshinamoorthy, A.; Asiri, A. M.; Garcia, H. Mixed-Metal or Mixed-Linker Metal Organic Frameworks as Heterogeneous Catalysts. *Catal. Sci. Technol.* **2016**, *6* (14), 5238−5261.
(20) Hillman, F.; Zimmerman, J. M.; Paek, S. M.; Hamid, M. R. A.; Lim, W. T.; Jeong, H. K. Rapid Microwave-Assisted Synthesis of Hybrid Zeolitic-Imidazolate Frameworks with Mixed Metals and Mixed Linkers. *J. Mater. Chem. A* **2017**, *5* (13), 6090−6099.
(21) Burrows, A. D. Mixed-Component Metal-Organic Frameworks (MC-MOFs): Enhancing Functionality through Solid Solution Formation and Surface Modifications. *CrystEngComm* **2011**, *13* (11), 3623−3642.
(22) Fernández-Luqueño, F.; López-Valdez, F.; Gamero-Melo, P.; Luna-Suárez, S.; Aguilera-González, E.; Martínez, A.; García-Guillermo, M.; Hernández-Martínez, G.; Herrera-Mendoza, R.; Álvarez-Garza, M.; Pérez-Velázquez, I. Heavy Metal Pollution in Drinking Water - a Global Risk for Human Health: A Review. *African J. Environ. Sci. Technol.* **2013**, *7* (7), 567−584.
(23) Bui, N. T.; Kang, H.; Teat, S. J.; Su, G. M.; Pao, C. W.; Liu, Y. S.; Zaia, E. W.; Guo, J.; Chen, J. L.; Meihaus, K. R.; Dun, C.; Mattox, T. M.; Long, J. R.; Fiske, P.; Kostecki, R.; Urban, J. J. A Nature-Inspired Hydrogen-Bonded Supramolecular Complex for Selective Copper Ion Removal from Water. *Nat. Commun.* **2020**, *11* (1), 3947.
(24) Demiral, H.; Güngör, C. Adsorption of Copper(II) from Aqueous Solutions on Activated Carbon Prepared from Grape Bagasse. *J. Clean. Prod.* **2016**, *124*, 103.
(25) Perić, J.; Trgo, M.; Vukojević Medvidović, N. Removal of Zinc, Copper and Lead by Natural Zeolite - A Comparison of Adsorption Isotherms. *Water Res.* **2004**, *38* (7), 1893.
(26) Wang, Y. Y.; Liu, Y. X.; Lu, H. H.; Yang, R. Q.; Yang, S. M. Competitive Adsorption of Pb(II), Cu(II), and Zn(II) Ions onto Hydroxyapatite-Biochar Nanocomposite in Aqueous Solutions. *J. Solid State Chem.* **2018**, *261*, 53.
(27) Zhou, L.; Li, N.; Owens, G.; Chen, Z. Simultaneous Removal of Mixed Contaminants, Copper and Norfloxacin, from Aqueous Solution by ZIF-8. *Chem. Eng. J.* **2019**, *362*, 628−637.
(28) Hoseini Rad, M.; Ghasemzadeh, M. A.; Sharif, M. S. Multi-Component Synthesis of Spiro[Indoline-3,4′-Pyrrolo[3,4-c]-Pyrazoles] Using Zn(BDC) Metal-Organic Frameworks as a Green and Efficient Catalyst. *Iran. Chem. Commun.* **2019**, *7* (4), 390−397.
(29) Buttersack, C. General Cluster Sorption Isotherm. *Microporous Mesoporous Mater.* **2021**, *316*, 110909.
(30) Niknam Shahrak, M.; Ghahramaninezhad, M.; Eydifarash, M. Zeolitic Imidazolate Framework-8 for Efficient Adsorption and Removal of Cr(VI) Ions from Aqueous Solution. *Environ. Sci. Pollut. Res.* **2017**, *24* (10), 9624−9634.
(31) Jiang, M.; Cao, X.; Liu, P.; Zhang, T.; Zhang, J. ZIF-8@ Polyvinylpyrrolidone Nanocomposites Based N-Doped Porous Carbon for Highly Efficient Oxygen Reduction Reaction in Alkaline Solution. *J. Electrochem. Soc.* **2016**, *163* (6), H459−H464.
(32) Ren, J.; Ledwaba, M.; Musyoka, N. M.; Langmi, H. W.; Mathe, M.; Liao, S.; Pang, W. Structural Defects in Metal−Organic Frameworks (MOFs): Formation, Detection and Control towards Practices of Interests. *Coord. Chem. Rev.* **2017**, *349*, 169−197.
(33) Shen, Y.; Li, W.; Wu, J.; Li, S.; Luo, H.; Dai, S.; Wu, W. Solvent Extraction of Lanthanides and Yttrium from Aqueous Solution with Methylimidazole in an Ionic Liquid. *Dalt. Trans.* **2014**, *43* (26), 10023−10032.
(34) Khan, N. A.; Hasan, Z.; Jhung, S. H. Adsorptive Removal of Hazardous Materials Using Metal-Organic Frameworks (MOFs): A Review. *J. Hazard. Mater.* **2013**, *244−245*, 444−456.
(35) Guan, T.; Li, X.; Fang, W.; Wu, D. Efficient Removal of Phosphate from Acidified Urine Using UiO-66 Metal-Organic Frameworks with Varying Functional Groups. *Appl. Surf. Sci.* **2020**, *501*, 144074.
(36) Ayawei, N.; Ebelegi, A. N.; Wankasi, D. Modelling and Interpretation of Adsorption Isotherms. *J. Chem.* **2017**, *2017*, 1.
(37) Kwon, S.; Fan, M.; DaCosta, H. F. M.; Russell, A. G.; Berchtold, K. A.; Dubey, M. K. *CO2 Sorption*; Elsevier Inc., 2011.
(38) Sun, S.; Yang, Z.; Cao, J.; Wang, Y.; Xiong, W. Copper-Doped ZIF-8 with High Adsorption Performance for Removal of Tetracycline from Aqueous Solution. *J. Solid State Chem.* **2020**, *285*, 121219.
(39) Bakhtiari, N.; Azizian, S. Adsorption of Copper Ion from Aqueous Solution by Nanoporous MOF-5: A Kinetic and Equilibrium Study. *J. Mol. Liq.* **2015**, *206*, 114−118.
(40) Lee, C. G.; Jeon, J. W.; Hwang, M. J.; Ahn, K. H.; Park, C.; Choi, J. W.; Lee, S. H. Lead and Copper Removal from Aqueous Solutions Using Carbon Foam Derived from Phenol Resin. *Chemosphere* **2015**, *130*, 59−65.
(41) Igberase, E.; Osifo, P.; Ofomaja, A. The Adsorption of Copper (II) Ions by Polyaniline Graft Chitosan Beads from Aqueous Solution: Equilibrium, Kinetic and Desorption Studies. *J. Environ. Chem. Eng.* **2014**, *2* (1), 362−369.
(42) Chen, J. J.; Ahmad, A. L.; Ooi, B. S. Poly(N-Isopropylacrylamide-Co-Acrylic Acid) Hydrogels for Copper Ion Adsorption: Equilibrium Isotherms, Kinetic and Thermodynamic Studies. *J. Environ. Chem. Eng.* **2013**, *1* (3), 339−348.

https://doi.org/10.1021/acsomega.2c00980
ACS Omega 2022, 7, 15862−15869

(43) Aluigi, A.; Tonetti, C.; Vineis, C.; Tonin, C.; Mazzuchetti, G. Adsorption of Copper(II) Ions by Keratin/PA6 Blend Nanofibres. *Eur. Polym. J.* **2011**, *47* (9), 1756−1764.
(44) Lee, Y. R.; Jang, M. S.; Cho, H. Y.; Kwon, H. J.; Kim, S.; Ahn, W. S. ZIF-8: A Comparison of Synthesis Methods. *Chem. Eng. J.* **2015**, *271*, 276−280.

https://doi.org/10.1021/acsomega.2c00980
ACS Omega 2022, 7, 15862−15869